ELSEVIER

Contents lists available at SciVerse ScienceDirect

Journal of Alloys and Compounds

journal homepage: www.elsevier.com/locate/jallcom



Rapid solidification of silver-rich Ag-Cu-Zr alloys

A. Castellero^{a,*}, D.H. Kang^{b,c}, I.-H. Jung^b, G. Angella^d, M. Vedani^e, M. Baricco^a

- ^a Dipartimento di Chimica I.F.M. and N.I.S., Università di Torino, Torino, Italy
- ^b Department of Mining and Materials Engineering, McGill University, Montreal, Quebec, Canada
- ^c Novelis Global Technology Center, Kingston, Ontario, Canada
- d Istituto per l'Energetica e le Interfasi, CNR-IENI, Milano, Italy
- e Dipartimento di Meccanica, Politecnico di Milano, Milano, Italy

ARTICLE INFO

Article history: Received 10 July 2011 Received in revised form 9 December 2011 Accepted 19 December 2011 Available online 27 December 2011

Keywords: Amorphous alloys Rapid solidification Ag-based alloys Calphad Microstructures

ABSTRACT

In this work we explored the possibility of obtaining amorphous/crystalline composites in the Ag-rich side of the Ag-Cu-Zr ternary system exploiting the presence of a miscibility gap in the liquid. Four alloys with nominal composition (at.%) $Ag_{75}Cu_{11}Zr_{14}$ (alloy A), $Ag_{73}Cu_{17}Zr_{10}$ (alloy B), $Ag_{47.5}Cu_{22.5}Zr_{30}$ (alloy C), $Ag_{47.5}Cu_{30}Zr_{22.5}$ (alloy D) were investigated. The effect of the cooling rate and the composition on phase selection and microstructures was evaluated by comparing slowly cooled master ingots and rapidly quenched ribbons. Evidence of the liquid miscibility gap was observed only in alloys B and D, either in the master ingots and the ribbons. After rapid solidification, partial amorphisation was achieved for alloys C and D, where precipitates of the Ag-rich solid solution, showing various sizes, are dispersed in the amorphous matrix. A significant increase in hardness was achieved in the case of partially amorphous ribbons of alloys C and D (442 HV and 533 HV, respectively). Experimental results are discussed on the basis of the recently reassessed ternary Ag-Cu-Zr phase diagram.

© 2011 Elsevier B.V. All rights reserved.

1. Introduction

It is well known that bulk metallic glasses (BMGs), or amorphous alloys, on the one hand are characterised by high yield strength and large elastic strain limit, and, on the other hand, they do not show plasticity in tension due to shear softening (i.e. plastic deformation occurring along bands with lowered viscosity) [1,2]. Improvement of the plastic deformation has been achieved, typically under a geometrical constraint (e.g. upon compression and bending), in BMG composites where second phase particles, such as ex situ ceramic particles [3], in situ coarse dendrites [4] or nanocrystalline precipitates [5–7], are homogeneously dispersed in the amorphous matrix.

The presence of a second phase (either amorphous or crystalline), forming a strong and intimate interface with the amorphous matrix, tends to promote the shear delocalisation by branching the individual shear bands and stops their propagation. The strain at failure of BMG composites strongly depends on the volume fraction, size, shape and distribution of the second phase inclusions. In the case of composites containing micron size ductile crystalline particles highly dispersed in the amorphous matrix, the shear band propagation is confined by the interparticle distance [4] and the ductile crystalline particles locally deform by dislocation mechanism [8], allowing plastic deformation either in compression

and tension [9]. Second phase inclusions with a spherical shape can further improve the plastic deformation of the composites with respect to dendritic precipitates, as shown in Ref. [10]. When the composite contains a fine dispersion of nanocrystalline particles, the initiation of multiple shear bands is promoted. However the shear band propagation is not inhibited because the particles size is of the same order of magnitude with respect to the shear band width [6,11].

In the last five years, an innovative approach for producing new types of BMG composites was developed exploiting the presence of a phase separation in the liquid state. This can be typically achieved by introducing one pair of elements with a positive enthalpy of mixing between them and a negative enthalpy of mixing with all the others. In this way amorphous/amorphous [12,13] and amorphous/crystalline [14,15] composites can be obtained. Amorphous/crystalline composites can be produced when one of the two immiscible liquids, with a reduced glass forming ability (GFA), tends to crystallise during cooling while the other liquid, having a higher GFA, is able to amorphise. Furthermore, different length scales in the microstructure can be produced depending on the transformation mechanism which occurs: interconnected fractal microstructures are the result of a continuous transformation such as the spinodal decomposition, whereas droplet-type microstructures result from a nucleation and growth mechanism [16].

In this paper we investigated the silver-rich corner of the Ag-Cu-Zr ternary system with the aim of obtaining amorphous/crystalline composites, exploiting the stable miscibility gap in the

^{*} Corresponding author. Tel.: +39 011 670 7097; fax: +39 011 670 7855. E-mail address: alberto.castellero@unito.it (A. Castellero).

liquid phase [17]. In fact, the Ag-rich liquid is expected to crystallise as ductile f.c.c.-Ag solid solution, whereas an amorphous matrix should form from the Ag-poor liquid, since complete glass formation was observed in the Cu–Zr–Ag system for Ag contents below 40 at.% [18,19]. The phase selection and the microstructures of four different alloys obtained at different cooling rates were interpreted on the basis of the recently reassessed ternary Ag–Cu–Zr phase diagram [17].

2. Experimental

Master alloy ingots with nominal composition (at.%) $Ag_{75}Cu_{11}Zr_{14}$ (alloy A), $Ag_{73}Cu_{17}Zr_{10}$ (alloy B), $Ag_{47.5}Cu_{22.5}Zr_{30}$ (alloy C), $Ag_{47.5}Cu_{30}Zr_{22.5}$ (alloy D) were prepared by arc melting the pure elements under Ar atmosphere. Each ingot was re-melted several times in order to obtain a good homogeneity. Rapid solidified ribbons (about $40~\mu m$ thick) were obtained by melt spinning using a wheel speed of 20~m/s in He atmosphere. Alloys A and B have a Ag content corresponding to 80~wt.% which is the minimum legal content for applications in jewellery.

A PANalytical X'Pert X-ray diffractometer (XRD) with Cu K_{α} radiation was used for structural characterisation. The microstructure of master alloys and as spun ribbons was observed with a Leica Stereoscan 410 scanning electron microscope (SEM) equipped with a energy dispersion spectroscopy (EDS) microprobe (Oxford Instruments). In some cases the metallographic samples were chemically etched with a solution containing 30% NH₄OH, 25% H₂O₂ and 45% CH₃CH₂OH after mirror polishing to 1 µm. The thermal stability of the as spun ribbons was characterised by differential scanning calorimetry at 20 K/min using a Diamond DSC Perkin Elmer. Hardness of the alloys was evaluated by instrumented indentation using a load controlled Fischerscope HM2000 with a Vickers diamond pyramid. For the master alloys and the as spun ribbons, indents with depth of 2 μ m were performed with a loading rate of 2 mN/s. In the case of the as spun ribbons, hardness profiles of the transversal section were obtained performing indents with depth of 0.2 µm along parallel rows at different distances from the ribbon surface. At least 8 measurements were performed for each series. For all the samples hardness values were extracted according to the standard ISO 14557-1. The capability of the ribbon to be plastically deformed was qualitatively estimated by bending test.

The thermodynamic calculations based on the CALPHAD technique [20] were performed using the FactSage software [21].

3. Results

Fig. 1(i) and (ii) shows the isopleths at 80 wt.% and 47.5 at.%, respectively. The predicted reaction sequence upon cooling of alloys A and C is the following

$$L \rightarrow L_1 + L_2$$
 (separation in two liquids) (1)

$$L_1 + L_2 \rightarrow L'_1 + L'_2 + \text{AgZr} (\text{primary precipitation})$$
 (2)

$$L'_1$$
 (Ag-rich) $\rightarrow L'_2$ (Ag-poor) + AgZr

$$+$$
 f.c.c.-Ag (monotectic reaction at \sim 900 $^{\circ}$ C) (3)

$$L_2'$$
 (Ag-poor) + f.c.c.-Ag \rightarrow AgZr

$$+ AgCu_4Zr (peritectic reaction at \sim 850 \,^{\circ}C)$$
 (4)

$$AgCu_4Zr + AgZr \rightarrow Cu_{10}Zr_7$$

$$+$$
 Ag (peritectoid reaction just above $600 \,^{\circ}$ C) (5)

In the case of alloys B and D, the sequence is similar to the previous one, except for reactions (2) and (3) that are respectively substituted by

$$L_1 + L_2 \rightarrow L'_1 + L'_2 + \text{AgCu}_4\text{Zr}(\text{primary precipitation})$$
 (2')

$$L'_1$$
 (Ag-rich) $\rightarrow L'_2$ (Ag-poor) + AgCu₄Zr

+ f.c.c.-Ag (monotectic reaction at
$$\sim 900 \,^{\circ}$$
C) (3')

The equilibrium phases predicted at room temperature for alloys A, C and D are f.c.c.-Ag, AgZr, $Cu_{10}Zr_7$, whereas those calculated for alloy B are f.c.c.-Ag, AgCu₄Zr, $Cu_{10}Zr_7$.

Fig. 2(i) shows the XRD patterns of the various master alloys. All the patterns show the presence of the crystallographic reflections

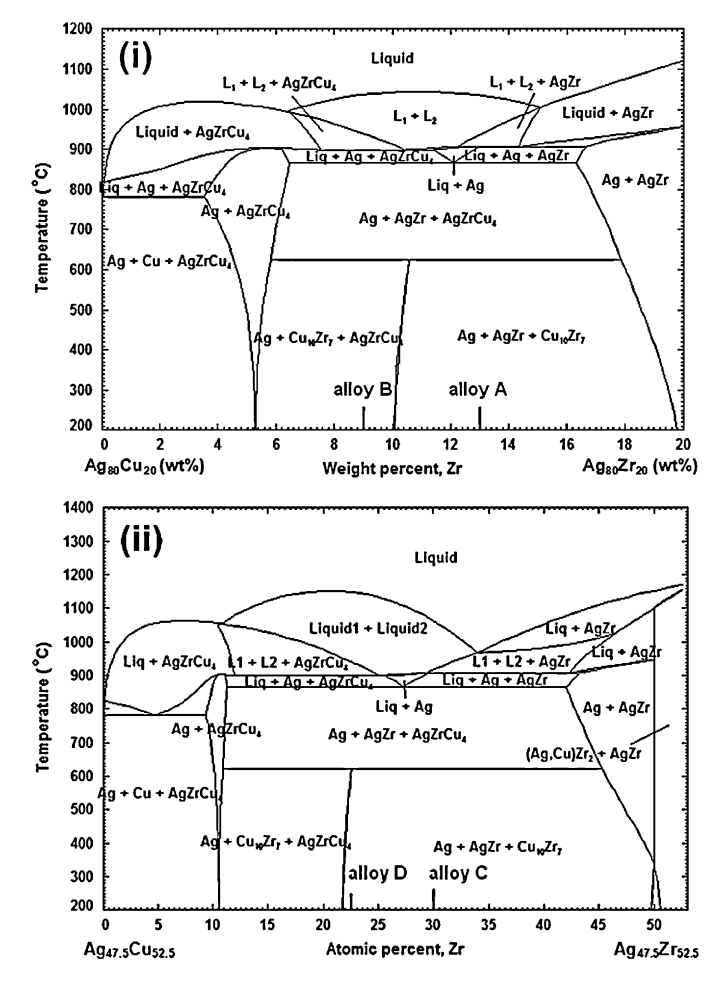


Fig. 1. Isopleths at 80 wt.% Ag (i) and 47.5 at.% Ag (ii) in the Ag–Cu–Zr system.

of the f.c.c.-Ag solid solution (dotted vertical lines). The remaining peaks were assigned to the following phases: AgZr and $\text{Cu}_{10}\text{Zr}_7$ in alloy A; $\text{Cu}_{10}\text{Zr}_7$, AgCu₄Zr (m-phase) in alloy B; AgZr in alloy C and in alloy D. For alloys C and D some XRD reflections could not be indexed.

The SEM micrographs of Fig. 3, obtained with the backscattered electrons signal, show the microstructures of the master alloys. In the case of alloy A, Fig. 3(i), the elongated needle of AgZr are the primary phase immersed in a matrix containing Ag and Cu₁₀Zr₇ formed during the monotectic reaction (3) and the peritectoid reaction (5), respectively. Fig. 3(ii), corresponding to alloy B, shows a droplet-type microstructure resulting from the phase separation in the liquid state; the bright phase corresponds to the f.c.c.-Ag solid solution, whereas in the dark droplets two different mixtures of intermetallic compounds were found: AgZr, Cu₁₀Zr₇ and AgCu₄Zr m-phase on the one hand (see top inset of Fig. 3(ii)) and AgCu₄Zr, AgZr, Cu₁₀Zr₇ and CuZr₂ on the other hand (see bottom inset of Fig. 3(ii)). The average composition of the dark droplets (about Cu₅₀Zr₃₀Ag₂₀ at.%), determined by EDS analysis, is similar in the whole sample independently of the microstructure. The microstructure of alloy C, Fig. 3(iii), shows bright dendrites of silver, resulting from the undercooling of the liquid, in a matrix containing lamellae of AgZr and the ternary AgCu₄Zr m-phase. After chemical etching, a fine microstructure containing Ag, AgZr and AgCu₄Zr is revealed at high magnification, as shown in the inset of Fig. 3(iii). In alloy D, Fig. 3(iv), the bright f.c.c.-Ag solid solution shows either a droplet like microstructure (see left inset of Fig. 3(iv)) and a dendritic microstructure (see right inset of Fig. 3(iv)). In the first case, the f.c.c.-Ag rich droplets are immersed in a coarse microstructure

Download English Version:

https://daneshyari.com/en/article/1615899

Download Persian Version:

https://daneshyari.com/article/1615899

<u>Daneshyari.com</u>